THE JOURNAL OF PHYSICAL CHEMISTRY Letters

pubs.acs.org/JPCL Letter

Structure, Stability, and Mechanical Properties of Boron-Rich Mo−B Phases: A Computational Study

Dmitry V. Rybkovskiy, Alexander G. Kvashnin,* Yulia A. Kvashnina, and Artem R. Oganov

Cite This: J. Phys. Chem. Lett. 2020, 11, 2393−2401 Read Online

ACCESS | Metrics & More | Article Recommendations | Supporting Information

ABSTRACT: Molybdenum borides were studied theoretically using first-principles calculations, parameterized lattice model, and global optimization techniques to determine stable crystal structures. Our calculations reveal the structures of known Mo−B phases, attaining close agreement with experiment. Following our developed lattice model, we describe in detail the crystal structure of boron-rich MoB_x phases with $3 \leq x \leq 9$ as the hexagonal $P6_3/mmc$-MoB_3 structure with Mo atoms partially replaced by triangular boron units. The most energetically stable arrangement of these B_3 units corresponds to their uniform distribution in the bulk, which leads to the formation of a disordered nonstoichiometric phase, with ordering arising at compositions close to $x = 5$ because of a strong repulsive interaction between neighboring B_3 units. The most energetically favorable structures of MoB_x correspond to the compositions $4 \lesssim x \leq 5$, with MoB_5 being the boron-richest stable phase. The estimated hardness of MoB_5 is 37−39 GPa, suggesting that the boron-rich phases are potentially superhard.

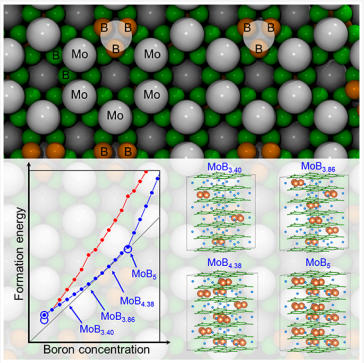

Transition metal borides are often considered as possible replacements of traditional superhard materials in various technological applications. Unlike widely used diamond and cubic boron nitride, transition metal borides do not require high pressure for their synthesis, making their production cheaper and more readily scalable. The outstanding mechanical properties of these materials originate from the combination of high valence electron density of metal atoms, responsible for high incompressibility, and covalent bonds of light boron atoms, resisting elastic and plastic shape deformations.[1,2] The borides of tungsten and molybdenum are of particular interest because of their capability to contain a significant amount of boron, resulting in high hardness. The W−B system has been extensively studied both experimentally[3−6] and theoretically,[7−9] whereas the exact crystal structure of higher Mo−B phases is still under debate.

Today, the experimental methods of structure determination are strongly supported by state-of-the-art computational techniques based on global optimization algorithms and robust quantum−chemical total energy computational methods.[10] Such approaches have already been applied to the investigation of the Mo−B phase diagram, shedding light on some aspects of the crystal structure of molybdenum borides. Liang et al.[11] computed the energies of the experimentally claimed and hypothetical crystal structures. Zhang et al.[12] used the evolutionary global optimization algorithm USPEX for an unbiased study of Mo−B phases. The latter work was, however, restricted to specific chemical compositions. Despite the success of the existing theoretical studies, the structure of the molybdenum borides with compositions close to MoB_4, which are particularly interesting for potential applications as hard materials, is still controversial. The experimentally proposed structures are mainly based on X-ray diffraction (XRD) experiments, where the largest part of the signal is determined by the positions of Mo atoms, and the correct placement of much lighter boron atoms is complicated. Total energy computations show that such structures have high energies of formation, indicating their instability.[11,12] On the other hand, the theoretically predicted $P6_3/mmc$-MoB_4 structure,[12] although having a low energy of formation, has an X-ray diffraction (XRD) pattern that is incompatible with experiment. These contraventions motivate a further search for boron-rich Mo−B phases that would match the experimental XRD and exhibit an energetically preferable boron arrangement.

In this work we use a broad range of computational techniques, including the evolutionary crystal structure prediction to search for thermodynamically stable phases through all possible compositions, density-functional total energy computations, and a parameterized lattice model for the theoretical study of the boron-rich part of the Mo−B phase diagram. We show that within the compositional range between MoB_4 and MoB_5, the molybdenum borides may be described by a structural model similar to the one proposed by

Received: January 23, 2020
Accepted: March 3, 2020
Published: March 3, 2020

https://dx.doi.org/10.1021/acs.jpclett.0c00242
J. Phys. Chem. Lett. 2020, 11, 2393−2401

Lech et al.[6] for the highest tungsten boride. On the basis of total energy computations and relative stabilities, we describe the requirements that the structures have to satisfy to be energetically preferable.

Global optimization of Mo−B crystal structures was performed using the variable-composition evolutionary algorithm as implemented in the USPEX code.[13−15] This approach makes it possible to perform an automatic structure search within the whole compositional range of a multicomponent system. During the structure search, the first generation of 120 structures was produced randomly with up to 24 atoms (for the variable-composition search) and 36 atoms (for the fixed-composition search) in the primitive cell. The succeeding generations were obtained by applying the heredity (40% of each generation), softmutation (20%), and transmutation (20%) operators;[13−15] 20% of each generation were produced using random[16] and random topological generators.[17]

For the structure relaxations and total energy computations, the projector augmented-wave[18,19] density functional theory (PAW-DFT) was used as implemented within the VASP[20−22] package. The generalized gradient approximation of Perdew−Burke−Ernzerhof (GGA-PBE)[23] was used for the exchange−correlation functional. PAW data sets were used to describe the electron−ion interactions with Mo 4p, 4d, 5s and B 2s, 2p electrons treated as valence electrons. The plane-wave energy cutoff of 400 eV, the Methfessel−Paxton electronic smearing,[24] and Γ-centered k-point meshes with a resolution of $2\pi \times 0.025$ Å^{-1} for the Brillouin zone sampling ensured the convergence of total energies.

To investigate the boron-rich part of the Mo−B phase diagram, a lattice model for the total energy was developed. X-ray diffraction has been simulated with the VESTA software[25] using 1.54059 Å wavelength.

Vickers hardness was estimated according to the Mazhnik−Oganov[26] (H_V^{MO}) and Chen[27] (H_V^{C}) models. Test calculations of Vickers hardness for a number of materials using Mazhnik−Oganov and Chen's models agree well with the reference experimental data: diamond, 99 and 94 GPa (~96 GPa[28]); TiN, 21 and 23 GPa (20.5 GPa[29]); and c-BN, 71 and 63 GPa (~66 GPa[30]).

Fracture toughness was calculated using the empirical Mazhnik−Oganov model[26] (K_{IC}^{MO}) and Niu−Oganov model[31] (K_{IC}). Calculated values of fracture toughness for well-studied materials nicely agree with experimental data. The Mazhnik−Oganov model gives 6.2, 7.7, 3.8, and 5.4 MPa·m$^{0.5}$ for diamond, WC, TiN, and c-BN, respectively. The Niu−Oganov model gives fracture toughness of diamond, WC, TiN, and c-BN equal to 6.3, 5.4, 3.3, and 5.4 MPa·m$^{0.5}$, respectively. The experimental data are 4−7 MPa·m$^{0.5}$ for diamond,[32−34] 5−8 MPa·m$^{0.5}$ for WC,[35,36] 3.5−5 MPa·m$^{0.5}$ for TiN,[35] and 2−5 MPa·m$^{0.5}$ for c-BN.[33,37]

Variable-Composition Evolutionary Structure Search. A thermodynamically stable phase has a lower energy of formation than any phase or phase assemblage of the same composition and is located on the convex hull line. The calculated energies of formation, ΔE_{form}, of the stable and metastable structures, obtained during evolutionary search and proposed earlier for some Mo−B phases in refs 3 and 38−41 are shown in Figure 1 as a function of the atomic fraction of boron.

The only stable phases obtained using the evolutionary search were $I4_1/amd$-MoB (α-MoB), $R\bar{3}m$-MoB_2, and $Pmmn$-MoB_5. It should be mentioned, however, that vibrational

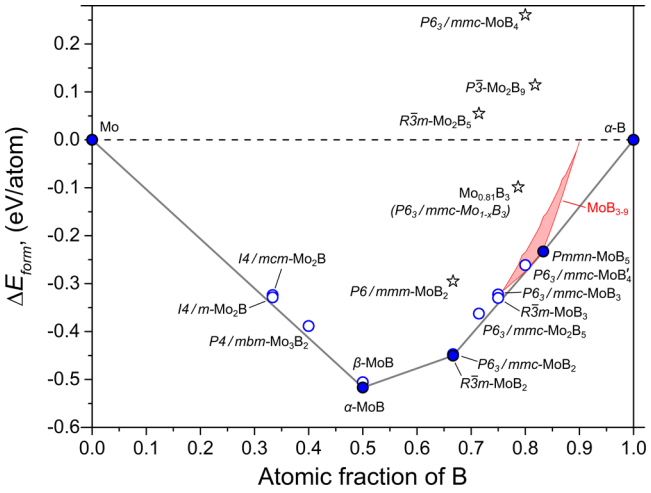

Figure 1. Calculated energies of formation in the Mo−B system. Filled and hollow circles designate stable and metastable phases, respectively. Stars show the energies of formation of the Mo−B structures proposed in the experimental works ($P6/mmm$-MoB_2,[38,42] $R\bar{3}m$-Mo_2B_5 [3], $P6_3/mmc$-$Mo_{0.81}B_3$ of the $Mo_{1-x}B_3$ type,[39] $P6_3/mmc$-MoB_4,[40] and $P\bar{3}$-Mo_2B_9 of the $W_{2-x}B_9$ type[41]). The shaded area depicts the energies of formation of boron-rich MoB_x phases with $3 \leq x \leq 9$, obtained using a parameterized lattice model.

effects might change the convex hull at high temperatures. Such vibrational contributions may result in stabilization of some phases close to the convex hull line. It is therefore important to consider not only systems lying on the convex hull in Figure 1, but also metastable phases, which are close to it. Such phases include $I4/m$-Mo_2B, $I4/mcm$-Mo_2B, $P4/mbm$-Mo_3B_2, $Cmcm$-MoB (β-MoB), $P6_3/mmc$-MoB_2, $P6/mmm$-MoB_2, $P6_3/mmc$-Mo_2B_5, $R\bar{3}m$-MoB_3, and $P6_3/mmc$-MoB_4', and further discussion on the basis of available experimental and theoretical data from literature will show that some of them may indeed become stable at finite temperature. Crystal structures of the USPEX-obtained Mo−B phases are shown in Figure 2. Each of the phases is discussed separately, starting from those having a low boron content.

The Mo_2B-phase is well known from experimental studies,[3,38,42,43] and global optimization predicts the $I4/mcm$ space group for this composition. However, it has been shown theoretically[44,45] that $I4/mcm$ phase is dynamically unstable and transforms to $I4/m$ phase. Total energy calculations of $I4/mcm$-Mo_2B and $I4/m$-Mo_2B show that they lie 20 and 16 meV/atom above the convex hull, respectively, which agrees with the previous theoretical findings.[11,12] Both structures are therefore metastable at 0 K, and we conclude that vibrational effects are responsible for the stabilization of Mo_2B. Another metastable structure, which has been experimentally found at high temperatures (T > 1550 K), is $P4/mbm$-Mo_3B_2, whose energy of formation lies 25 meV/atom above the convex hull. It was first reported by Steinitz et al. in 1952,[38] though some later works doubted its existence.[42]

We also obtained two known MoB phases: $I4_1/amd$-MoB (α-MoB) and $Cmcm$-MoB (β-MoB). The energy of formation of β-MoB is higher than that of α-MoB by 11 meV/atom. $I4_1/amd$-MoB undergoes a phase transition to the high-temperature $Cmcm$-MoB at ~1900 K, as known from experiment and predicted by theory.[11,38,42]

The chemical compositions and crystal structures of boron-rich Mo−B phases were debated for a long time. We obtained

https://dx.doi.org/10.1021/acs.jpclett.0c00242
J. Phys. Chem. Lett. 2020, 11, 2393−2401

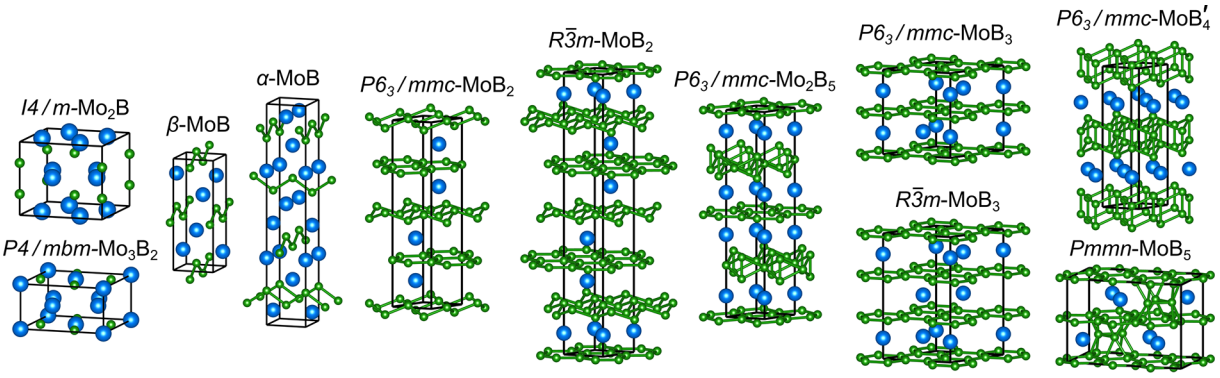

Figure 2. Crystal structures of the Mo−B phases obtained using the evolutionary crystal structure search.

Table 1. Mechanical Properties of the Low-Energy Mo−B Phases

phase	B, GPa	G, GPa	E, GPa	ν	H_V^C, GPa	H_V^{MO}, GPa	H_V^{exp}, GPa	K_{IC}, MPa·m$^{0.5}$	K_{IC}^{MO}, MPa·m$^{0.5}$
$I4_1/amd$-MoB	308	203	500	0.229	24.5	23.2	23.0[38]	3.9	4.2
$Cmcm$-MoB	307	193	478	0.241	22.1	21.9	24.5[38]	3.2	4.1
$R\bar{3}m$-MoB_2	299	230	548	0.193	32.4	30.3	24.2[49]	4.7	4.2
$R\bar{3}m$-MoB_3	267	222	522	0.175	34.9	33.2		4.9	3.9
$P6_3/mmc$-MoB_3	269	225	527	0.173	35.5	33.8		4.7	3.9
$Pmmn$-MoB_5	264	232	538	0.16	38.6	37.3		5.6	3.8

two low-energy structures for MoB_2: $R\bar{3}m$-MoB_2 and $P6_3/mmc$-MoB_2 (Figure 1). The synthesis of MoB_2 having the AlB_2-type structure ($P6/mmm$ space group)[42] was first reported by Steinitz et al.[38] Later studies by Higashi et al.[46] reported the $R\bar{3}m$ phase. Our calculations show that the energy of $P6/mmm$-MoB_2 is higher by 152 meV/atom compared to that of $R\bar{3}m$-MoB_2, which agrees with the previous theoretical studies.[11,12] The structure of $P6_3/mmc$-MoB_2 corresponds to the $hP12$-WB_2 type proposed in ref 11 and lies 3 meV/atom above the lowest-energy $R\bar{3}m$-MoB_2.

Mo_2B_5 was reported in several experimental works[3,38,42] and was first described by Kiessling[3] as a derivative of the $R\bar{3}m$-MoB_2 structure with alternating planar hexagonal and puckered (with additional B atoms) hexagonal boron layers separated by Mo layers.[3,43] The existence of this phase has been questioned by experiments,[46,47] and a conclusion has been made that it actually is identical to $R\bar{3}m$-MoB_2. Later, another metastable, lower-energy $P6_3/mmc$-Mo_2B_5 with a different structure was predicted theoretically.[12] We found that $R\bar{3}m$-Mo_2B_5 is unstable, having a positive energy of formation of 55 meV/atom, and $P6_3/mmc$-Mo_2B_5 is 25 meV/atom above the convex hull, which agrees with the previous theoretical results.[11,12]

We found that $R\bar{3}m$-MoB_3 is metastable, lying 12 meV/atom above the convex hull, which agrees with the previous theoretical results. In comparison, $P6_3/mmc$-MoB_3 differs by the mutual position of the hexagonal Mo layers, and its calculated energy is 7 meV/atom higher, but previous theoretical investigations have suggested that it becomes more stable than the $R\bar{3}m$ phase at high temperatures.[11]

The MoB_4 structure with $P6_3/mmc$ space group, which we denote as the $P6_3/mmc$-MoB_4' phase, is metastable, lying 15 meV/atom above the convex hull. This phase is equivalent to those obtained in previous theoretical global optimization studies.[12] It is composed of Mo layers sandwiched between puckered boron bilayers. Numerous experimental works reported the synthesis of boron-rich compounds with compositions close to MoB_4.[39,40,48] However, the structures proposed in these works have a different XRD pattern in comparison to the theoretical $P6_3/mmc$-MoB_4' phase.

Our evolutionary structure search revealed a new stable boron-rich phase $Pmmn$-MoB_5 with the same structure type as that of an earlier reported WB_5.[8] This phase is made of edge- and face-sharing MoB_{12} hexagonal prisms and open B_{15} clusters linked into a 3D structure by B−B bonds. The calculated phonon spectrum shows the dynamical stability of this phase (Supporting Information Figure S3). Crystal structures of all low-energy phases are presented in Table S1.

Because the main practical interest in boron-rich molybdenum borides is due to their potential for technological applications as hard materials, we estimated the mechanical properties of the obtained low-energy Mo−B phases. The results are summarized in Table 1. The Vickers hardness, estimated using the Chen (H_V^C)[27] and Mazhnik−Oganov (H_V^{MO})[26] models, is in good agreement with the experimental values for α-MoB and β-MoB,[38] whereas some overestimation is observed in the case of the $R\bar{3}m$-MoB_2 phase.[49] The estimated hardness values for MoB_3 are ∼33−36 GPa. For the most boron-rich phase $Pmmn$-MoB_5, we estimated the Vickers hardness as ∼37−39 GPa, which is close to the lower bound for superhard materials, 40 GPa.[29,50,51] Therefore, the highest borides of molybdenum are potentially superhard. It is worth noting that a recent experimental study of boron-rich molybdenum boride with the composition $Mo_{0.757}B_3$ reported anisotropic nanoindentation hardness of ∼34−40 GPa.[53] A comparison of mechanical characteristics with known materials is shown in Figure S1 (see the Supporting Information).

Higher Molybdenum Borides. Our variable-composition evolutionary search reproduced most of the experimentally observed phases and predicted the boron-richest phase MoB_5 that has not been reported experimentally. There have been several experimental reports of Mo−B phases with the composition close to MoB_4 and a controversial structure determination,[39,40,48] whereas the evolutionary search did not find any structures of MoB_4 that would match the experimentally observed XRD pattern.

https://dx.doi.org/10.1021/acs.jpclett.0c00242
J. Phys. Chem. Lett. 2020, 11, 2393−2401

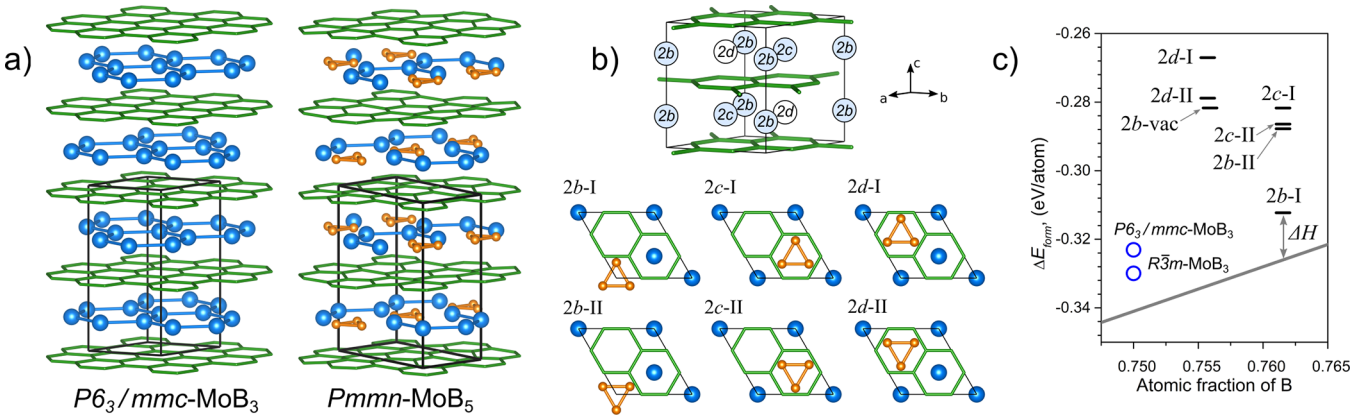

Figure 3. (a) Crystal structures of $P6_3/mmc$-MoB_3 and $Pmmn$-MoB_5. To make the structure of each layer clear, the interlayer space is shown enlarged. The molybdenum atoms are shown as large blue circles. The hexagonal sheets of boron are depicted as a green wireframe. The boron atoms forming the triangular units are displayed in orange. (b) Unit cell of $P6_3/mmc$-MoB_3 with the Wyckoff positions where a B_3 unit can be placed. Below, the top view of a single layer of MoB_3 with a B_3 unit placed in different positions and orientations. (c) Energies of formation of 2 × 2 × 2 supercells with the B_3 unit in different configurations, together with a single Mo vacancy in the 2*b* position (2*b*-vac). The convex hull is shown as a solid gray line connecting MoB_2 and MoB_5.

Crystal structures in the boron-rich area of the Mo−B phase diagram are difficult to study experimentally because of a large difference in the X-ray scattering cross sections of boron and metal atoms which makes it hard to determine the exact positions of boron atoms and the boron content in the compound. Previous proposals for several structures of boron-rich Mo−B compounds have been made mainly on the basis of chemical intuition and limited experimental data. These structures usually consist of sequences of hexagonal graphene-like boron and molybdenum layers with partial Mo occupancies and additional boron fragments of different forms. However, theoretical total energy computations showed that these hypothetical structures have high energies of formation, indicating their instability. Galasso and Pinto[40] proposed the $P6_3/mmc$-MoB_4 phase with boron dimers placed between the hexagonal boron layers and oriented along the *c* axis of a unit cell. After relaxation of this structure, we obtained a positive energy of formation of 261 meV/atom, which agrees with previous theoretical works.[11,12] Another structure, suggested by Lundström and Rosenberg,[39] has $Mo_{1-x}B_3$ composition with $x \approx 0.20$ and $P6_3/mmc$ space group. This structure is similar to $P6_3/mmc$-MoB_3, obtained during the USPEX evolutionary search, but with a portion of Mo atoms removed. To simulate this structure, we constructed a 2 × 2 × 1 supercell of $P6_3/mmc$-MoB_3 with three Mo vacancies in the Wyckoff position 2*b*, which resulted in the composition $Mo_{0.8125}B_3$. Its energy of formation is negative, −98 meV/atom, but lying quite high above the convex hull (Figure 1), which makes this structure unstable. A recent experimental work considered a similar structure with $Mo_{0.757}B_3$ composition.[53] We also examined the experiment-based structure of Nowotny et al.[41] for higher tungsten borides. This structure with the composition $Mo_{2-x}B_9$ features boron octahedra and lacks one of the two hexagonal graphene-like boron layers. After relaxation of Mo_2B_9 structure, the atoms significantly rearranged, but the resulting energy of formation remained positive at 114 meV/atom (Figure 1). We conclude that crystal structures proposed on the basis of the experimental measurements are unstable. Although the positions of metal atoms can be robustly determined from XRD, constructing an energetically favorable arrangement of light boron atoms is extremely complicated. Experiment-independent structure prediction approaches have also been used before to resolve the correct crystal structure of boron-rich phases. The computations have revealed the $P6_3/mmc$-MoB_4' phase[12] that also appeared in our global optimization procedure. This structure has a low energy of formation and is located only 15 meV/atom above the convex hull. However, its XRD pattern is distinctly different from that of the experimentally synthesized highest molybdenum boride.[39,40,48] Similar puzzle existed in the chemically similar W−B system. In 2015, Lech et al. carried out neutron diffraction studies of boron-rich W−B phases,[6] partially replacing the tungsten atoms in the Wyckoff position 2*b* with boron trimers, which resulted in $WB_{4.2}$ chemical composition having $P6_3/mmc$ space group. It should be noted that recent teoretical work considered the equilibrium arrangement of these boron trimers within the $WB_{4.2}$ crystal.[52] However, our global optimization procedure did not reveal such structures with partial atomic occupations because of the limited unit cell size used in the evolutionary search (up to 36 atoms per unit cell). At the same time, it is possible to construct the energetically favorable Mo−B phases that have the compositions between MoB_4 and MoB_5 by analyzing the structures of USPEX-predicted phases.

The crystal structures of $P6_3/mmc$-MoB_3 and $Pmmn$-MoB_5 (Figure 3a) have clear similarities: the alternation of graphene-like boron layers with the layers of Mo. The structure of MoB_5 can be produced from MoB_3 by replacing half of the Mo atoms in the Wyckoff position 2*b* by three boron atoms in a triangular arrangement (a B_3 unit), shown in orange in Figure 3a. This agrees with the structure proposed by Lech et al.[6] We considered the possibility to construct stable MoB_x phases having various compositions by replacing a different number of Mo atoms with boron triangles.

We first focused on the preferable position and orientation of an individual boron triangle. In the $P6_3/mmc$-MoB_3 structure, such B_3 units may occupy three Wyckoff positions: 2*b*, 2*c*, and 2*d* (Figure 3b). To reveal the most favorable position and orientation of a B_3 unit, we constructed a 2 × 2 × 2 supercell of $P6_3/mmc$-MoB_3 and placed a single B_3 unit at these Wyckoff positions, either replacing the molybdenum atom at the corresponding site or filling an empty space of the Wyckoff position 2*d* (Figure 3b). The two Mo layers in the

https://dx.doi.org/10.1021/acs.jpclett.0c00242
J. Phys. Chem. Lett. 2020, 11, 2393−2401

$P6_3/mmc$-MoB_3 unit cell differ in rotation by $\frac{\pi}{3}$; therefore, we considered the B_3 units in only one of these layers, keeping in mind that a change of layer would require a proper rotation of the boron triangle. We also considered a supercell with a single Mo vacancy in the 2*b* position for comparison, because some of the experimentally suggested Mo−B phases have partial occupation of the Mo sublattice due to vacancies.[39,53] We relaxed the atomic coordinates and lattice parameters of the resulting supercells and evaluated their total energies using DFT. The distance above the convex hull ΔH was used as a quantitative measure to compare the relative stabilities of the structures. The resulting energies of formation as a function of composition are shown in Figure 3c, and the energy values are summarized in Table 2. Most of the B_3 configurations, as well as a single Mo vacancy, have higher ΔH than the initial $P6_3/mmc$-MoB_3. The instability of the Mo vacancy is consistent with the high energy of formation of the $Mo_{0.8125}B_3$ structure, discussed above. The most stable configuration was realized when a boron triangle replaced a Mo atom in the Wyckoff position 2*b* so as to maximize the distance to the closest in-plane Mo atoms (2*b*-I configuration). This most preferred B_3 configuration results in the lowering of ΔH compared to pure $P6_3/mmc$-MoB_3 from 18 to 14 meV/atom. Therefore, there is a prospect for the structure stabilization by replacement of more Mo atoms in the Wyckoff positions 2*b* and a consequent increase in the B_3 content. Such increase in the boron concentration would bring the energies of formation of the resulting structures closer to the convex hull line. However, as the number of B_3 units increases, the distance between them becomes smaller, their mutual position starts to play a role, and the interaction between the individual B_3 units has to be considered.

Table 2. Energies of Formation and Energy above the Convex Hull (ΔH) for 2 × 2 × 2 Supercells of $P6_3/mmc$-MoB_3 with Different Locations of the B_3 Unit and Mo Vacancy in the 2*b* Position

structure type	E_{form} (meV/atom)	ΔH (meV/atom)
$P6_3/mmc$-MoB_3	−323	18
2*b*-I	−312	14
2*b*-II	−288	38
2*c*-I	−282	44
2*c*-II	−286	40
2*d*-I	−267	67
2*d*-II	−279	55
2*b*-vac	−274	44
Pmmn-MoB_5	−233	0

The investigation of possible mutual arrangements of B_3 units requires consideration of many configurations with large supercells, complicating the computations that use the first-principles DFT approach. To approximate the DFT results, we developed a lattice model that is very accurate for the boron-rich Mo−B compounds. In this model, the Wyckoff positions 2*b* of $P6_3/mmc$-MoB_3 are considered as lattice sites that may be occupied by either Mo atoms or B_3 units in the 2*b*-I configuration. The total energy of a supercell consisting of *N* unit cells of $P6_3/mmc$-MoB_3 with $0 \le n \le 2N$ B_3 units (there are 2*N* possible sites for the placement of B_3 units because an individual $P6_3/mmc$-MoB_3 unit cell contains two Mo layers) can be approximately expressed as

$$E_{N,n} = NE_{MoB_3} + n\Delta E_{B_3} + \frac{1}{2}\sum_{i\neq j} K_{ij}s_i s_j \quad (1)$$

In this formula, E_{MoB_3} is the energy of a single $P6_3/mmc$-MoB_3 unit cell. ΔE_{B_3} is the energy change produced by the replacement of a single Mo atom by a B_3 unit in its lowest-energy configuration, calculated as the total energy difference between a 2 × 2 × 2 supercell of $P6_3/mmc$-MoB_3 with a B_3 unit in the 2*b*-I configuration and a pristine 2 × 2 × 2 $P6_3/mmc$-MoB_3 supercell. The first two energy terms serve as the definition of the absolute energy value and may differ depending on the particular DFT implementation used. The third term represents the interaction between the individual B_3 units located in the 2*b* sites *i* and *j*, where K_{ij} is a parameter whose value depends on the distance between the sites that are occupied by the B_3 units. The interactions up to the fourth nearest-neighbor site were taken into account. Each 2*b* site has two nearest neighbors located above and below along the *c* axis. Six second-order neighbors are located in the same layer plane. Twelve third-order neighbors occupy the upper and lower planes of 2*b* sites. The two remaining neighbors of the fourth order are located along the *c* axis at a distance twice as long as the first-order neighbors. The graphical representation of the neighbor map is shown in Figure S4. s_i is equal to 1 or 0 if the *i*th site is occupied by a B_3 unit or a Mo atom, respectively.

Thus, six parameters completely describe our lattice model, with two of them, obtained from the energies of 2 × 2 × 2 supercells, defining the absolute energy. Four remaining parameters, responsible for the B_3 interaction, were fit to reproduce the DFT total energies of supercells with multiple B_3 units. To do this, we constructed 18 2 × 2 × 2 and 14 2 × 2 × 3 supercells with randomly distributed B_3 units, having the compositions between $MoB_{3.4}$ and $MoB_{5.23}$. We calculated their total energies within the DFT approach and then minimized the squared difference between the DFT energies and lattice model energies from eq 1 with use of the random walk minimization procedure. The resulting set of parameters is presented in Table 3. All parameters responsible for the interaction have positive values, which indicates the repulsive nature of the B_3−B_3 interaction. For the supercells constructed for the fitting procedure, the largest absolute difference between the total energy calculated using the DFT and our lattice model was ∼1 meV/atom. By construction, the highest accuracy of our lattice model is attained for boron-poor systems, diminishing as the boron content increases (the largest error in the total energy was 12 meV/atom for the MoB_9 structure).

Table 3. Interaction Parameters Used for Calculating the Total Energies within the Lattice Model (1)

neighbor order	number of neighbors	distance	*K* (eV)
1	2	*c*/2	1.289
2	6	*a*	0.095
3	12	$\sqrt{a^2 + c^2/4}$	0.019
4	2	*c*	0.103

Having accurately parameterized the lattice model, we searched for the most stable composition, corresponding to the optimal arrangement of the B_3 units, by considering the 2 × 2 × 3 $P6_3/mmc$-MoB_3 supercell and performing a brute-force

https://dx.doi.org/10.1021/acs.jpclett.0c00242
J. Phys. Chem. Lett. 2020, 11, 2393−2401

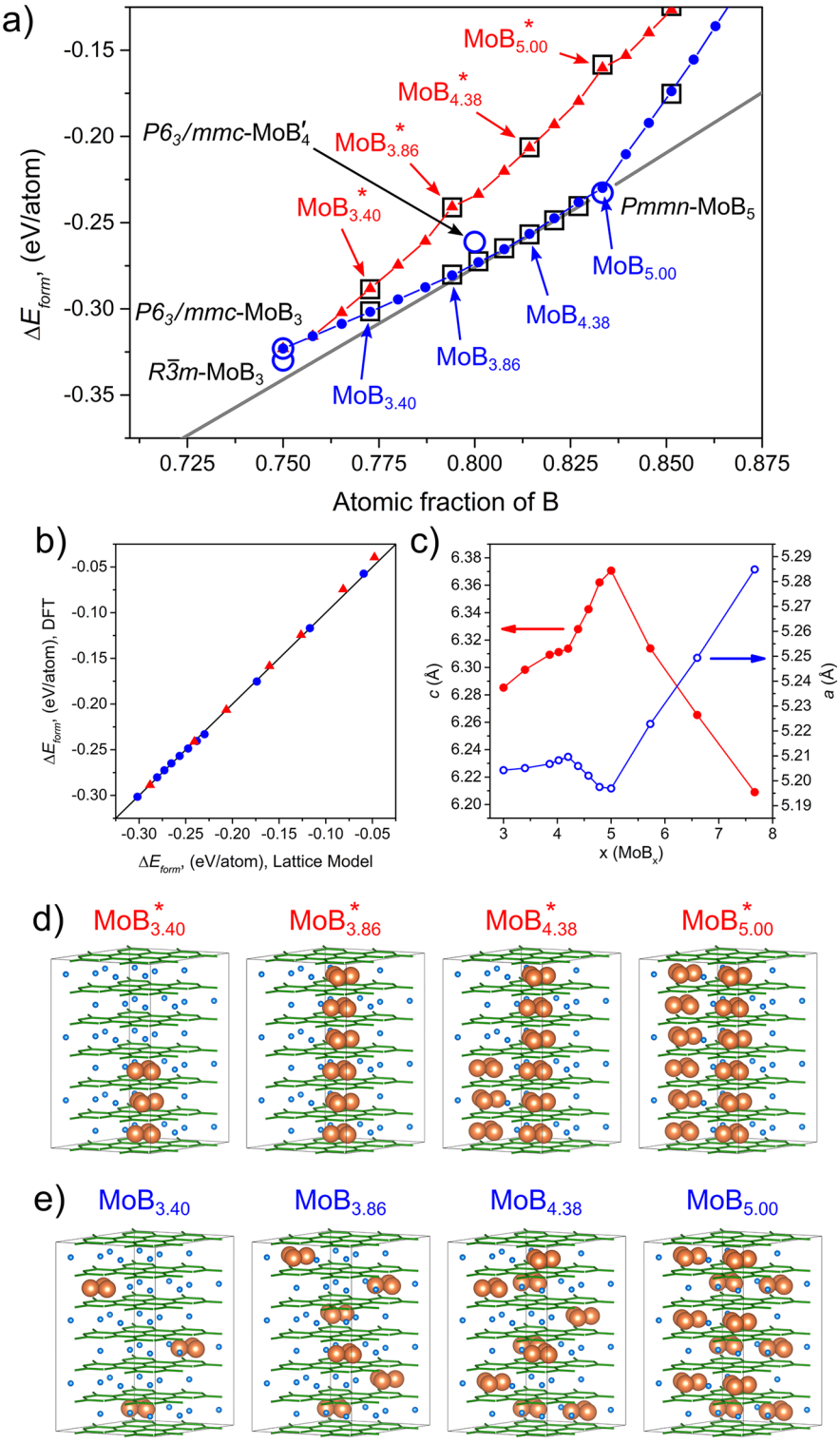

Figure 4. (a) Energies of formation of boron-rich MoB_{3-9} structures. A gray line depicts the convex hull. Structures obtained during the evolutionary global search are shown as open circles. The lowest- and highest-energy structures obtained using the lattice model are shown as small blue circles and red triangles, respectively. Open squares show the energies of structures recalculated within the DFT. (b) Comparison between the energies of formation for the most and least stable MoB_x phases, obtained within the lattice model and recalculated within DFT. (c) Dependence of the equilibrium lattice constants per single $P6_3/mmc$ primitive cell on the composition of the low-energy MoB_x phases. (d) Selected structures with the highest energy of formation showing the energetically unfavorable columns of the B_3 units. The boron atoms forming the triangular units are displayed in orange. (e) Lowest-energy structures of the same compositions. The B_3 units are uniformly distributed in the bulk of a crystal.

search for lowest-energy structures, taking into account all possible arrangements of the B_3 units. The energies of formation of the constructed nonstoichiometric structures are shown in Figure 4a, displaying only the boron-rich region of the convex hull diagram from Figure 1. An increase in the boron content leads to a decrease in the energy of formation,

https://dx.doi.org/10.1021/acs.jpclett.0c00242
J. Phys. Chem. Lett. 2020, 11, 2393−2401

which approaches the convex hull line at the composition close to MoB_4 (within the 2 × 2 × 3 supercell approach, the obtained composition is $MoB_{4.02}$, lying just 2 meV/atom above the convex hull) and closely follows this line until the composition MoB_5 on the convex hull is reached. Taking into account the effects of lattice vibrations and configurational entropy will make this phase stable. Further increase in the boron content leads to a rapid decrease in stability (the energy of formation increases). The composition range between $4 \lesssim x \leq 5$ is therefore the most stable within the considered structure type, with MoB_5 being the most boron-rich among them. To verify the accuracy of the obtained results, we recalculated the energy of formation of some structures within DFT. The corresponding energies of formation, marked by squares in Figure 4a, show excellent agreement between the lattice model and DFT calculations (a direct comparison between the results of the lattice model and DFT is shown in Figure 4b). Figure 4c shows the dependence of the equilibrium lattice constants (per single $P6_3/mmc$ primitive cell) on the boron content of the lowest-energy MoB_x phases. Such dependence could be used for experimental determination of the chemical composition of these compounds, by experimentally calibrating the dependence of the cell parameters on the composition. The plot clearly shows different behavior at different boron concentrations. In the range from MoB_3 to $MoB_{4.2}$, the addition of more B_3 units leads to a small increase of both lattice constants a and c. For structures between $MoB_{4.2}$ and MoB_5, which correspond to the interval of the most stable compositions, the parameter c increases from 6.31 to 6.37 Å with a small decrease of lattice constant a from 5.21 to 5.20 Å. Further increase of the boron content results in an opposite trend, with a fast decrease of the c parameter and increase of a.

During the brute-force search, we collected the data on the highest-energy structures to determine the origins of the energy penalty due to the arrangement of B_3 units. Crystal structures of the least and most stable phases are shown in Figure 4d,e to clearly see the structural difference between them. In the low-energy structures (Figure 4e), the B_3 units, shown in orange, are uniformly distributed within the considered cells, whereas in the high-energy structures (Figure 4d), the B_3 units tend to form vertical columns. The high energy of these structures is the consequence of the repulsion between the B_3 units, which also explains the jump in the energy for structures where tatomic fraction of boron is greater than 5/6. MoB_5 is the boron-richest phase where the B_3 units can be distributed without being placed in the adjacent sites. This is the highest theoretically achievable molybdenum boride within the proposed type. The lowest-energy B_3 arrangements, presented in Figure 4e, are not unique. Multiple different configurations, corresponding to the ground-state energies, were found during our brute-force search, which points at the disordered nature of this material. However, at the MoB_5 composition, the strong repulsive interaction between the nearest-neighbor B_3 units reduces the number of lowest-energy configurations and suggests the ordering of B_3 units at compositions close to MoB_5.

Our calculations show that the MoB_x structures, constructed via partial replacement of the 2b-Mo atoms of the $P6_3/mmc$-MoB_3 phase by triangular B_3 units, are energetically more preferable than the previously proposed boron-rich Mo−B phases with compositions close to MoB_4, including $P6_3/mmc$-MoB_4' (see Figure 4a) and $P6_3/mmc$-$Mo_{1-x}B_3$ (see Figures 1 and 3c and ref 39). We compared the simulated X-ray diffraction patterns of these molybdenum borides (Figure 5). The XRD pattern of $P6_3/mmc$-MoB_4' (Figure 5a) is clearly

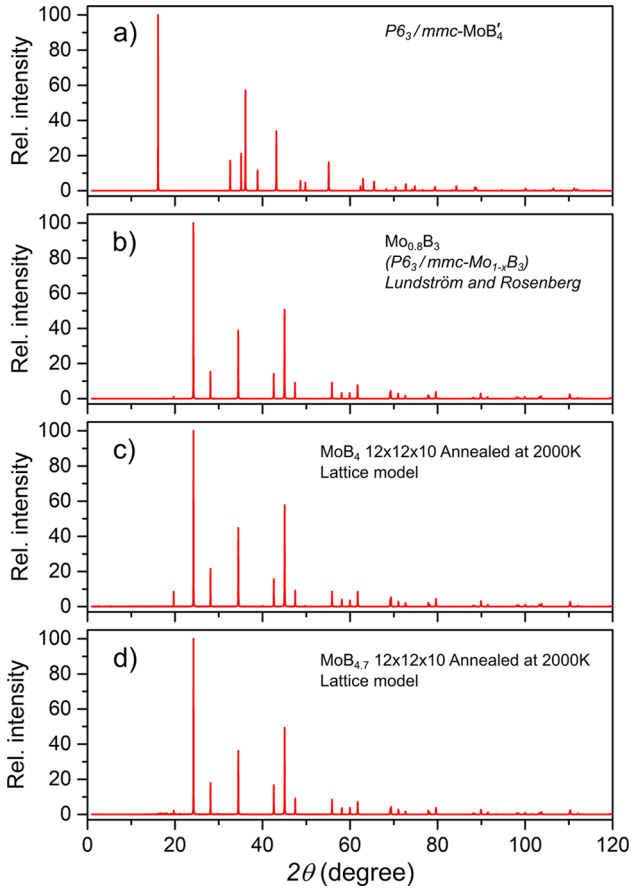

Figure 5. Simulated XRD spectra. (a) Previously theoretically proposed $P6_3/mmc$-MoB_4'. (b) Experimentally proposed $P6_3/mmc$-$Mo_{1-x}B_3$ model[39] with x = 0.2. (c) MoB_4 and (d) $MoB_{4.7}$ structures, constructed as 12 × 12 × 10 supercells of the $P6_3/mmc$-MoB_3 phase, with a partial replacement of the Mo atoms in the 2b-position by B_3 units.

different from the most widely accepted $P6_3/mmc$-$Mo_{1-x}B_3$ (x = 0.20) model (Figure 5b), proposed experimentally and closely reproducing experimental XRD pattern.[39] Given that both lattice parameters and XRD peak intensities are very sensitive to the exact stoicheometry (see Figure 4d and Figure 5c,d), the agreement with experiment for both the XRD peak intensities and the predicted lattice parameters corresponding to the composition $MoB_{4.7}$ suggests that the actual chemical composition of samples studied in ref 39 is close to $MoB_{4.7}$. To obtain the XRD pattern of the MoB_x phases within our suggested structure type, we considered a 12 × 12 × 10 supercell using our lattice model (1) and performed an annealing of the B_3 positions at 2000 K with the Metropolis Monte Carlo algorithm to simulate the high-temperature synthesis conditions. The resulting XRD pattern for the MoB_4 composition (Figure 5c) is in good agreement with the experimental model. The main difference between them is related to the peak at 19.7°, the intensity of which is determined the value of the fractional occupation of the Mo atoms in the 2b position. The replacement of a larger fraction of Mo atoms with B_3 units, which leads to the composition of $MoB_{4.7}$ (Figure 5d), allowed us to decrease the relative

https://dx.doi.org/10.1021/acs.jpclett.0c00242
J. Phys. Chem. Lett. 2020, 11, 2393−2401

intensity of this peak, bringing the resulting XRD spectrum in closer agreement with experiment. Further increase of boron content resulted in the appearance of additional peaks at around 18° in the simulated XRD pattern because of the B_3 units ordering. Such ordering appears because of the strong repulsive interaction between the B_3 units, located at the adjacent sites, which restricts the number of their possible arrangements.

Good agreement between the experimental XRD pattern[39] and the XRD pattern of our proposed structure, together with its favorable thermodynamics, gives strong evidence in favor of this structure (which can be described as based on the $P6_3/mmc$ -MoB_3 structure with partial replacement of Mo atoms in the 2*b*-position with triangular B_3 units). Our calculations show that the highest theoretically achievable molybdenum boride within this structure type is MoB_5.

In conclusion, the crystal structure of boron-rich Mo−B phases has been debated for a long time. The structural complexity of pure boron manifests itself in the boron-rich part of the transition metal boride phase diagram. In this work we used a range of computational approaches, including the evolutionary global optimization, first-principles total energy calculations, and a parameterized lattice model, to investigate the atomic structures of Mo−B phases in the whole compositional range. Beside the phases reported and characterized in previous experimental and theoretical studies, we found a new stable phase of MoB_5, having the same structure type as previously predicted WB_5.[8] We showed that the appropriate mixing of structural fragments of MoB_5 and metastable $P6_3/mmc$-MoB_3 (the partial replacement of the molybdenum atoms in the Wyckoff position 2*b* by appropriately rotated boron triangles B_3) makes it possible to construct a broad range of structures with the compositions between MoB_3 and MoB_9. The development and application of a lattice model for total energy calculations allowed us to find energetically stable boron-rich phases with MoB_4−MoB_5 compositions. The energetically favorable MoB_x phases correspond to a uniform distribution of the B_3 units within the hexagonal lattice, based on the tendency of these units to avoid each other in the bulk. The crystal structure of MoB_x with low concentrations of B_3 units is disordered and similar to those proposed by Lech et al.[6] for the W−B system. An increase in the boron content decreases spatial freedom for boron triangles because of the repulsive interaction neighboring B_3 units, resulting in their ordering at compositions close to MoB_5. The estimations of Vickers hardness show that higher borides have a high hardness of 33−39 GPa, indicating the possible superhardness of these materials. In addition, we showed that the computational structure prediction methods are powerful tools for determining the structure of systems in situations where an experimental crystal structure assessment is complicated.

■ ASSOCIATED CONTENT

Supporting Information

The Supporting Information is available free of charge at https://pubs.acs.org/doi/10.1021/acs.jpclett.0c00242.

Crystal data, mechanical properties, physical properties of MoB_5, and lattice model neighbor map (PDF)

■ AUTHOR INFORMATION

Corresponding Author

Alexander G. Kvashnin − *Skolkovo Institute of Science and Technology, Skolkovo Innovation Center, Moscow 121205, Russia; Moscow Institute of Physics and Technology, Dolgoprudny 141700, Russia;* orcid.org/0000-0002-0718-6691; Email: A.Kvashnin@skoltech.ru

Authors

Dmitry V. Rybkovskiy − *Skolkovo Institute of Science and Technology, Skolkovo Innovation Center, Moscow 121205, Russia; A. M. Prokhorov General Physics Institute of RAS, Moscow 119991, Russia*

Yulia A. Kvashnina − *Pirogov Russian National Research Medical University, Moscow 117997, Russia*

Artem R. Oganov − *Skolkovo Institute of Science and Technology, Skolkovo Innovation Center, Moscow 121205, Russia; Moscow Institute of Physics and Technology, Dolgoprudny 141700, Russia; International Center for Materials Discovery, Northwestern Polytechnical University, Xi'an 710072, China;* orcid.org/0000-0002-9315-1419

Complete contact information is available at: https://pubs.acs.org/10.1021/acs.jpclett.0c00242

Notes

The authors declare no competing financial interest.

■ ACKNOWLEDGMENTS

This work was supported by the Russian Science Foundation (No. 19-72-30043). The calculations were carried out on Rurik supercomputer at MIPT and Arkuda and Pardus supercomputers of the Skolkovo Foundation.

■ REFERENCES

(1) Kaner, R. B.; Gilman, J. J.; Tolbert, S. H. Designing Superhard Materials. *Science* **2005**, *308* (5726), 1268−1269.

(2) Levine, J. B.; Tolbert, S. H.; Kaner, R. B. Advancements in the Search for Superhard Ultra-Incompressible Metal Borides. *Adv. Funct. Mater.* **2009**, *19* (22), 3519−3533.

(3) Kiessling, R.; et al. The Crystal Structures of Molybdenum and Tungsten Borides. *Acta Chem. Scand.* **1947**, *1* (10), 893−916.

(4) Romans, P. A.; Krug, M. P. Composition and Crystallographic Data for the Highest Boride of Tungsten. *Acta Crystallogr.* **1966**, *20* (2), 313−315.

(5) Itoh, H.; Matsudaira, T.; Naka, S.; Hamamoto, H.; Obayashi, M. Formation Process of Tungsten Borides by Solid State Reaction between Tungsten and Amorphous Boron. *J. Mater. Sci.* **1987**, *22* (8), 2811−2815.

(6) Lech, A. T.; Turner, C. L.; Mohammadi, R.; Tolbert, S. H.; Kaner, R. B. Structure of Superhard Tungsten Tetraboride: A Missing Link between MB_2 and MB_{12} Higher Borides. *Proc. Natl. Acad. Sci. U. S. A.* **2015**, *112* (11), 3223−3228.

(7) Cheng, X.-Y.; Chen, X.-Q.; Li, D.-Z.; Li, Y.-Y. Computational Materials Discovery: The Case of the W−B System. *Acta Crystallogr., Sect. C: Struct. Chem.* **2014**, *70* (2), 85−103.

(8) Kvashnin, A. G.; Zakaryan, H. A.; Zhao, C.; Duan, Y.; Kvashnina, Y. A.; Xie, C.; Dong, H.; Oganov, A. R. New Tungsten Borides, Their Stability and Outstanding Mechanical Properties. *J. Phys. Chem. Lett.* **2018**, *9* (12), 3470−3477.

(9) Zhao, C.; Duan, Y.; Gao, J.; Liu, W.; Dong, H.; Dong, H.; Zhang, D.; Oganov, A. R. Unexpected Stable Phases of Tungsten Borides. *Phys. Chem. Chem. Phys.* **2018**, *20* (38), 24665−24670.

(10) Oganov, A. R.; Pickard, C. J.; Zhu, Q.; Needs, R. J. Structure Prediction Drives Materials Discovery. *Nat. Rev. Mater.* **2019**, *4* (5), 331−348.

(11) Liang, Y.; Yuan, X.; Fu, Z.; Li, Y.; Zhong, Z. An Unusual Variation of Stability and Hardness in Molybdenum Borides. *Appl. Phys. Lett.* **2012**, *101* (18), 181908.
(12) Zhang, M.; Wang, H.; Wang, H.; Cui, T.; Ma, Y. Structural Modifications and Mechanical Properties of Molybdenum Borides from First Principles. *J. Phys. Chem. C* **2010**, *114* (14), 6722−6725.
(13) Oganov, A. R.; Glass, C. W. Crystal Structure Prediction Using *Ab Initio* Evolutionary Techniques: Principles and Applications. *J. Chem. Phys.* **2006**, *124* (24), 244704.
(14) Oganov, A. R.; Ma, Y.; Lyakhov, A. O.; Valle, M.; Gatti, C. Evolutionary Crystal Structure Prediction as a Method for the Discovery of Minerals and Materials. *Rev. Mineral. Geochem.* **2010**, *71* (1), 271−298.
(15) Oganov, A. R.; Lyakhov, A. O.; Valle, M. How Evolutionary Crystal Structure Prediction Works—and Why. *Acc. Chem. Res.* **2011**, *44* (3), 227−237.
(16) Lyakhov, A. O.; Oganov, A. R.; Stokes, H. T.; Zhu, Q. New Developments in Evolutionary Structure Prediction Algorithm USPEX. *Comput. Phys. Commun.* **2013**, *184* (4), 1172−1182.
(17) Bushlanov, P. V.; Blatov, V. A.; Oganov, A. R. Topology-Based Crystal Structure Generator. *Comput. Phys. Commun.* **2019**, *236*, 1−7.
(18) Blöchl, P. E. Projector Augmented-Wave Method. *Phys. Rev. B: Condens. Matter Mater. Phys.* **1994**, *50* (24), 17953−17979.
(19) Kresse, G.; Joubert, D. From Ultrasoft Pseudopotentials to the Projector Augmented-Wave Method. *Phys. Rev. B: Condens. Matter Mater. Phys.* **1999**, *59* (3), 1758−1775.
(20) Kresse, G.; Hafner, J. Ab Initio Molecular Dynamics for Liquid Metals. *Phys. Rev. B: Condens. Matter Mater. Phys.* **1993**, *47* (1), 558−561.
(21) Kresse, G.; Hafner, J. Ab Initio Molecular-Dynamics Simulation of the Liquid-Metal–Amorphous-Semiconductor Transition in Germanium. *Phys. Rev. B: Condens. Matter Mater. Phys.* **1994**, *49* (20), 14251−14269.
(22) Kresse, G.; Furthmüller, J. Efficient Iterative Schemes for Ab Initio Total-Energy Calculations Using a Plane-Wave Basis Set. *Phys. Rev. B: Condens. Matter Mater. Phys.* **1996**, *54* (16), 11169−11186.
(23) Perdew, J. P.; Burke, K.; Ernzerhof, M. Generalized Gradient Approximation Made Simple. *Phys. Rev. Lett.* **1996**, *77* (18), 3865−3868.
(24) Methfessel, M.; Paxton, A. T. High-Precision Sampling for Brillouin-Zone Integration in Metals. *Phys. Rev. B: Condens. Matter Mater. Phys.* **1989**, *40* (6), 3616−3621.
(25) Momma, K.; Izumi, F. VESTA3 for Three-Dimensional Visualization of Crystal, Volumetric and Morphology Data. *J. Appl. Crystallogr.* **2011**, *44* (6), 1272−1276.
(26) Mazhnik, E.; Oganov, A. R. A Model of Hardness and Fracture Toughness of Solids. *J. Appl. Phys.* **2019**, *126* (12), 125109.
(27) Chen, X.-Q.; Niu, H.; Li, D.; Li, Y. Modeling Hardness of Polycrystalline Materials and Bulk Metallic Glasses. *Intermetallics* **2011**, *19* (9), 1275−1281.
(28) Andrievski, R. A. Superhard Materials Based on Nanostructured High-Melting Point Compounds: Achievements and Perspectives. *Int. J. Refract. Hard Met.* **2001**, *19* (4), 447−452.
(29) Stone, D. S.; Yoder, K. B.; Sproul, W. D. Hardness and Elastic Modulus of TiN Based on Continuous Indentation Technique and New Correlation. *J. Vac. Sci. Technol., A* **1991**, *9* (4), 2543−2547.
(30) *The Science of Hardness Testing and Its Research Applications*; Westbrook, J. H., Conrad, H., Eds.; American Society for Metals: Cleveland, OH, 1973.
(31) Niu, H.; Niu, S.; Oganov, A. R. Simple and Accurate Model of Fracture Toughness of Solids. *J. Appl. Phys.* **2019**, *125* (6), 065105.
(32) Drory, M. D.; Dauskardt, R. H.; Kant, A.; Ritchie, R. O. Fracture of Synthetic Diamond. *J. Appl. Phys.* **1995**, *78* (5), 3083−3088.
(33) Brookes, C. A. The Mechanical Properties of Cubic Boron Nitride. *Sci. Hard Mater. Proc. Int. Conf.* **1986**.
(34) Irifune, T.; Kurio, A.; Sakamoto, S.; Inoue, T.; Sumiya, H. Ultrahard Polycrystalline Diamond from Graphite. *Nature* **2003**, *421* (6923), 599−600.
(35) Munro, R. G.; Freiman, S. W.; Baker, T. L. *Fracture Toughness Data for Brittle Materials*; NIST, 1998.
(36) Groover, M. P. *Fundamentals of Modern Manufacturing: Materials, Processes, and Systems*; John Wiley & Sons, 2010.
(37) Solozhenko, V. L.; Kurakevych, O. O.; Le Godec, Y. Creation of Nanostuctures by Extreme Conditions: High-Pressure Synthesis of Ultrahard Nanocrystalline Cubic Boron Nitride. *Adv. Mater.* **2012**, *24* (12), 1540−1544.
(38) Steinitz, R.; Binder, I.; Moskowitz, D. System Molybdenum-Boron and Some Properties of The Molybdenum-Borides. *JOM* **1952**, *4* (9), 983−987.
(39) Lundström, T.; Rosenberg, I. The Crystal Structure of the Molybdenum Boride Mo1−xB3. *J. Solid State Chem.* **1973**, *6* (2), 299−305.
(40) Galasso, F.; Pinto, J. Metal Borides in Boron Fiber Cores: Identefication of MoB4. *Trans Met Soc. AIME* **1968**, *242*, 754.
(41) Nowotny, H.; Haschke, H.; Benesovsky, F. Bor-reiche Wolframboride. *Monatsh. Chem.* **1967**, *98* (3), 547−554.
(42) Spear, K. E.; Liao, P. K. The B−Mo (Boron-Molybdenum) System. *Bull. Alloy Phase Diagrams* **1988**, *9* (4), 457−466.
(43) Kiessling, R.; et al. The Borides of Some Transition Elements. *Acta Chem. Scand.* **1950**, *4*, 209−227.
(44) Zhou, D.; Wang, J.; Cui, Q.; Li, Q. Crystal Structure and Physical Properties of Mo2B: First-Principle Calculations. *J. Appl. Phys.* **2014**, *115* (11), 113504.
(45) Wang, M.; Liu, C.; Wen, M.; Li, Q.; Ma, Y. Investigations on Structural Determination of Semi-Transition-Metal Borides. *Phys. Chem. Chem. Phys.* **2017**, *19* (47), 31592−31598.
(46) Higashi, I.; Okada, S.; Takahashi, Y. Crystal Structure of MoB2. *J. Less-Common Met.* **1986**, *123*, 277−283.
(47) Frotscher, M.; Klein, W.; Bauer, J.; Fang, C.-M.; Halet, J.-F.; Senyshyn, A.; Baehtz, C.; Albert, B. M2B5 or M2B4? A Reinvestigation of the Mo/B and W/B System. *Z. Anorg. Allg. Chem.* **2007**, *633* (15), 2626−2630.
(48) Chretien, A.; Helgorsky, J. On New Boride Compositions of Molybdenum and Tungsten, MoB4 and WB4. *CR (East Lansing, MI)* **1961**, *252* (5), 742−744.
(49) Okada, S.; Atoda, T.; Higashi, I.; Takahashi, Y. Preparation of Single Crystals of MoB2 by the Aluminium-Flux Technique and Some of Their Properties. *J. Mater. Sci.* **1987**, *22* (8), 2993−2999.
(50) Solozhenko, V. L.; Gregoryanz, E. Synthesis of Superhard Materials. *Mater. Today* **2005**, *8* (11), 44−51.
(51) Solozhenko, V. L.; Kurakevych, O. O.; Andrault, D.; Le Godec, Y.; Mezouar, M. Ultimate Metastable Solubility of Boron in Diamond: Synthesis of Superhard Diamondlike ${\mathrm{BC}}_{5}$. *Phys. Rev. Lett.* **2009**, *102* (1), 015506.
(52) Gong, W.; Liu, C.; Song, X.; Li, Q.; Ma, Y.; Chen, C. Unravelling the Structure and Strength of the Highest Boride of Tungsten $WB_{4.2}$. *Phys. Rev. B: Condens. Matter Mater. Phys.* **2019**, *100* (22), 220102.
(53) Tang, H.; Gao, X.; Zhang, J.; Gao, B.; Zhou, W.; Yan, B.; Li, X.; Zhang, Q.; Peng, S.; Huang, D.; et al. Boron-Rich Molybdenum Boride with Unusual Short-Range Vacancy Ordering, Anisotropic Hardness, and Superconductivity. *Chem. Mater.* **2020**, *32*, 459.

https://dx.doi.org/10.1021/acs.jpclett.0c00242
J. Phys. Chem. Lett. 2020, 11, 2393−2401